iScience

Article

Differentiation of human pluripotent stem cells into urothelial organoids via transient activation of WNT signaling

Graphical abstract

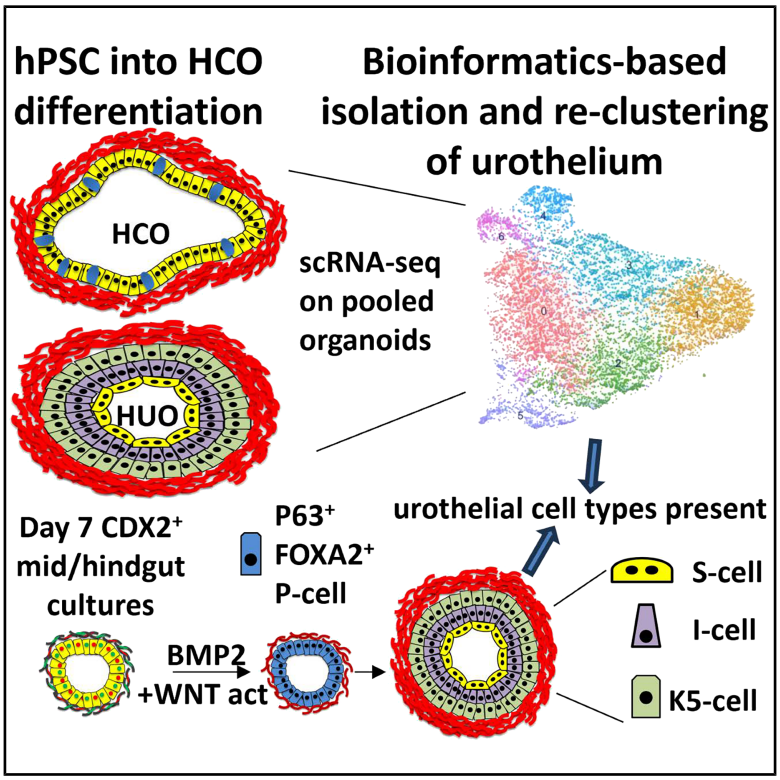

Highlights

- WNT signaling is higher in the ventral versus dorsal cloaca of mice
- WNT signaling promotes urothelial differentiation of human hindgut cultures
- HUOs contain urothelial cell types and display barrier function
- HUO development mirrors early mammalian urothelial development

Authors

Na Qu, Abdelkader Daoud, Daniel O. Kechele, Cassie E. Cleary, Jorge O. Múnera

Correspondence

munera@musc.edu

In brief

Molecular Genetics; Stem cells research; Developmental biology

Qu et al., 2025, iScience *28*, 112398
May 16, 2025
https://doi.org/10.1016/j.isci.2025.112398

CellPress

iScience

CellPress
OPEN ACCESS

Article

Differentiation of human pluripotent stem cells into urothelial organoids via transient activation of WNT signaling

Na Qu,[1] Abdelkader Daoud,[1] Daniel O. Kechele,[2] Cassie E. Cleary,[1] and Jorge O. Múnera[1,3,*]
[1]Department of Regenerative Medicine and Cell Biology, Medical University of South Carolina, Charleston, SC 29425, USA
[2]Division of Developmental Biology, Cincinnati Children's Hospital Medical Center, Cincinnati, OH 45229-3039, USA
[3]Lead contact
*Correspondence: munera@musc.edu
https://doi.org/10.1016/j.isci.2025.112398

SUMMARY

The cloaca is a transient structure that forms in the terminal hindgut giving rise to the rectum dorsally and the urogenital sinus ventrally. Similarly, human hindgut cultures derived from human pluripotent stem cells generate human colonic organoids (HCOs) which also contain co-developing urothelial tissue. In this study, our goal was to identify pathways involved in cloacal patterning and apply this to human hindgut cultures. RNA sequencing (RNA-seq) data comparing dorsal versus ventral cloaca in e10.5 mice revealed that WNT signaling was elevated in the ventral versus dorsal cloaca. Inhibition of WNT signaling in hindgut cultures maintained their differentiation toward colonic organoids. WNT activation promoted differentiation toward human urothelial organoids (HUOs). HUOs contained developmental stage specific cell types present in mammalian urothelial tissue including co-developing mesenchyme. Therefore, HUOs offer a powerful *in vitro* model for dissecting the regulatory pathways that control the dynamic emergence of stage specific cell types within the human urothelium.

INTRODUCTION

The epithelia of the small intestine, colorectum, and urothelium are derived from the definitive endoderm. The urothelial epithelium is derived from the ventral portion of the cloaca which forms in the terminal hindgut.[1] The cloaca undergoes septation resulting in the separation of the urogenital sinus (UGS) from the colorectum. Improper septation of the cloaca can result in anorectal malformations (ARMs), a common pathology affecting approximately 1 in 5,000 births.[2] Despite the frequency of ARMs, the mechanisms underlying their development remain poorly understood. This is partly attributed to the absence of appropriate *in vitro* models.

The generation of transplantable urothelial tissue remains an urgent medical need. Patients with bladder cancer,[3] interstitial cystitis,[4] and bladder exstrophy[5] often require bladder replacement. The standard of care for all of these patients is construction of neobladder from tissue derived from the patient's own ileum or sigmoid colon,[6] a procedure which has a high rate (27%) of complications.[7] Expansion of autologous urothelial progenitors could be a source of replacement tissue. However, in the case of bladder cancer, these progenitors may have oncogenic mutations making them unsuitable for transplantation. Urethral injuries due to blunt trauma can lead to complications such as impotence or incompetence.[8,9] Therefore, generation of urothelial tissues from human pluripotent stem cells could provide a continuous source of urothelium that could be used for tissue replacement.

We previously developed a method to generate human colonic organoids (HCOs) from human pluripotent stem cells by inducing hindgut patterning. Recently, we demonstrated that by increasing the plating density of the starting cultures, we could generate HCOs with co-developing macrophages. In addition, we also observed urothelium in these cultures.[10] In this study, we identified wingless-type MMTV integration site family (WNT) signaling as a pathway that is upregulated in the ventral portion of the cloaca in mice. We found that WNT signaling inhibition prevented urothelial differentiation while WNT signaling activation enhanced urothelial differentiation. HUOs generated by activation of WNT signaling contained basal, intermediate, and luminal urothelial cells. HUOs were stratified even in the absence of exogenous factors. In addition, HUOs contained mesenchymal cell types that are present in human urothelial tissues. Therefore, HUOs provide an *in vitro* platform for studying human urothelial development.

RESULTS

Genome wide transcriptomic analysis reveals the presence of urothelial-like cell types in HCO cultures

Analysis of RNA sequencing (RNA-seq) data from H1 embryonic stem cells (ESCs) derived human intestinal organoids (HIOs) and HCOs (Figure S1A), revealed the presence of urothelial transcripts within HCO cultures but not HIO cultures (Figure S1B). This indicates that the bone morphogenetic protein BMP signaling that

is required for the specification of HCOs, also specified urothelial tissue, which is consistent with the known role of BMP signaling in posterior-ventral development.[11–15] We confirmed the presence of urothelial tissue expressing GATA3 which is expressed in human adult bladder, an endoderm derived urothelial tissue.[16] We also examined the expression of KRT13, which marks the transitional epithelium of the human bladder but not the epithelium of the small intestine or colon.[17] We found that urothelial organoids developed in similar numbers to colonic organoids (Figures 1A, 1B, S1C, and S1D). In addition, we found a small subset of organoids that expressed both urothelial and colonic markers (Figures S1C and S1D). These results demonstrate that HCO cultures contain co-developing urothelium.

To determine the cellular diversity of urothelial cells within H1 ESC derived 22-day-old and 37-day-old HCO cultures, we bioinformatically selected the urothelial endoderm from single cell RNA sequencing (scRNA-seq) data from HCO cultures. Uniform manifold approximation and projection (UMAP) analysis of urothelial endoderm revealed the presence of 7 different cell populations within the urothelium including previously described superficial cells (S-cells) and basal keratin 5 expressing cells (K5-cells)[18,19] (Figures 1C and 1D, Table S1). Although we saw an induction of *KRT14* mRNA in 35-day-old HCO cultures in the bulk RNA-seq data (Figure S1B), we did not detect basal *KRT14* expressing cells (K14-cells) in the scRNA-seq data (Figure S1E). In addition, we found that the urothelial cells followed a similar developmental trajectory to what occurs in mice since *KRT5* expressing cells were not apparent in 22-day-old organoids but present in 37-day-old organoids (Figures 1C–1E). In summation, these data demonstrate that HCO cultures contain diverse urothelial cell types including urothelial progenitors that undergo maturation and differentiation.

RNA-seq profiling of dorsal and ventral cloaca reveals patterning and increased WNT signaling in the ventral region

To improve the differentiation of HCO cultures toward urothelial tissues, we determined the signaling pathways and transcription factors that are differentially enriched in the ventral versus dorsal cloaca. To achieve this, we analyzed a publicly available dataset from the GenitoUrinary Development Molecular Anatomy Project (GUDMAP). In this dataset, the ventral and dorsal cloaca from e10.5 mouse embryos was separated using laser capture microdissection and subjected to RNA-seq analysis. Principal-component analysis (PCA) revealed that ventral and dorsal cloaca samples clustered into distinct groups based on their transcriptomic profiles (Figure S2A). We then performed gene ontology analysis on transcripts that were enriched in ventral versus dorsal cloaca (Table S2). Consistent with the known role of WNT signaling in the induction of urothelial identity,[20–22] we found a strong enrichment for WNT signaling in the ventral cloaca (Figure S2B), indicating that there is differential WNT signaling activity in the ventral versus dorsal cloaca, consistent with previous studies.[20,23] Gene ontology analysis of dorsal cloaca revealed a strong enrichment for epithelial development and embryonic morphogenesis (Figure S3A).

To examine the transcription factors that are enriched in the ventral cloaca, we filtered out the transcription factors present in the differentially expressed genes. We observed enrichment of several transcripts known to be enriched in bladder tissue (which is urothelial) including *Trp63*[24,25] and GATA binding protein 3 (*Gata3*)[26] (Figure S2C). Dorsal cloaca was enriched in colon transcription factors including caudal type homeobox 2 *Cdx2*[27,28] and the intestinal mesenchyme marker NK2 homeobox 3 (*Nkx2-3*)[29,30] (Figure S3B). Wholemount immunofluorescence staining of e10–10.5 mouse embryos revealed that TP63, GATA3, and runt related transcription factor 1 (RUNX1) were all expressed in the ventral portion of the posterior hindgut while CDX2 was expressed in the dorsal portion of the posterior hindgut (Figures S2D–S2F, Video S1). GATA3 also stained other tissues which are known to express GATA3 including the nephric ducts (which are derived from mesoderm), consistent with previous studies,[31–34] and confirming the specificity of our staining. Our findings reveal that WNT signaling is elevated in the ventral cloaca compared to the dorsal cloaca and that CDX2, TP63, GATA3, and RUNX1 are differentially expressed in the dorsal versus ventral portion of the posterior hindgut.

Transient WNT activation in human hindgut cultures promotes differentiation into urothelial organoids

Based on the data from mice, we determined if WNT signaling could pattern HCO cultures along the dorsal-ventral axis. To do this, we patterned IPSC72.3[35] derived organoids using BMP2 but also treated, either with an inhibitor of catenin related transcription 3 (ICRT3), or the glycogen synthase kinase 3 (GSK3) inhibitor CHIR99021 (CHIR) from days 7–10 (Figure 2A). PCA of the RNA-seq data revealed that WNT inhibited and WNT activated samples clustered into distinct groups based on their transcriptomic profiles (Figure 2B). Gene ontology analysis on transcripts that were enriched in WNT activated organoids (Table S3), revealed an enrichment for proliferation associated genes and a significant enrichment for WNT signaling and skeletal system development (Figure 2C). WNT inhibited organoids were enriched in circulatory system development and tube development (Figure S3C, Table S3). Analysis of transcription factors revealed that WNT inhibition resulted in the increased expression of several factors known to be involved in colorectal development, such as H2.0 like homeobox (HLX),[36] or expressed specifically in intestinal tissue such as intestine specific homeobox (ISX).[37] (Figure S3D). In contrast, WNT activation resulted in the increased mRNA expression of several factors known to be involved in urothelial development including grainyhead like transcription factor 3 GRHL3[38] and tumor protein p63 (TP63)[24] (Figure 3D). Furthermore, 5 of the top 10 transcription factors that were upregulated in WNT-activated day 10 hindgut cultures (Figure 3D), were also upregulated in the ventral cloaca including ALX homeobox 4 (*ALX4*), distal-less homeobox 5 (*DLX5*), *DLX6*, msh homeobox 2 (*MSX2*), and *TP63*.

To determine if urothelial cells were generated from CDX2+ endoderm from our IPSC72.3 derived mid/hindgut cultures, we performed immunostaining for CDX2 and TP63. Although TP63 is expressed in other endoderm tissues including the esophagus and trachea,[39] these other tissues are not derived from CDX2+ mid/hindgut. Consistent with previous studies,[40,41] we found that the endoderm (as marked by forkhead box A2 (FOXA2)) in our mid/hindgut cultures expressed CDX2 exclusively. CDX2 expression was maintained in day 10 ICRT3 organoids but was

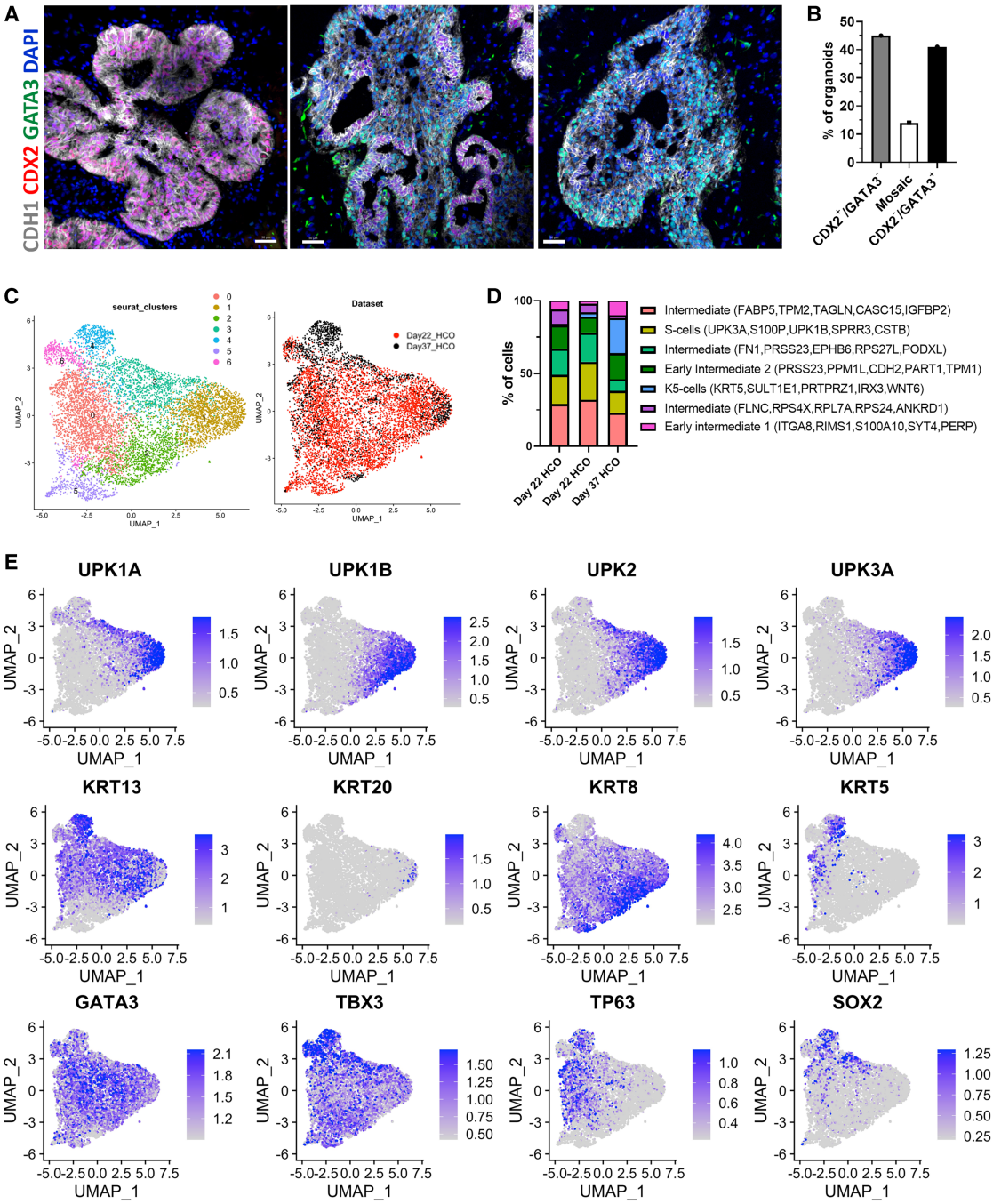

Figure 1. Urothelial tissue is present in HCO differentiations

(A and B) (A) Immunofluorescence staining and (B) quantification on day 35 H1 ESC derived HCOs for CDH1 (white), CDX2 (red), and GATA3 (green) and counterstained with DAPI (blue). A total of 29 organoids from 3 separate differentiations were analyzed.

(C) Uniform manifold approximation and projection (UMAP) Seurat clustering of all urothelial cells from the d22 and d37 HCO cultures.

(D) Relative proportions of predicted cell types as well as corresponding markers in each HCO sample.

(E) Feature plots of select urothelial genes including uroplakin genes (*UPK1A*, *1B*, *2*, and *3A*), keratin genes (*KRT13*, *20*, *8*, and *5*) and transcription factors (*GATA3*, *TBX3*, *TP63*, and *SOX2*). See also Figure S1 and Table S1. Scale bars: (A) 50 μm.

decreased in day 10 CHIR treated organoids (Figures 2E and 2F). Instead, the day 10 CHIR treated organoids expressed TP63 (Figures 2E and 2F). These results indicate that WNT signaling promotes the differentiation of human hindgut cultures into TP63+ urothelial progenitors that give rise to the epithelium in human urothelial organoids (HUOs).

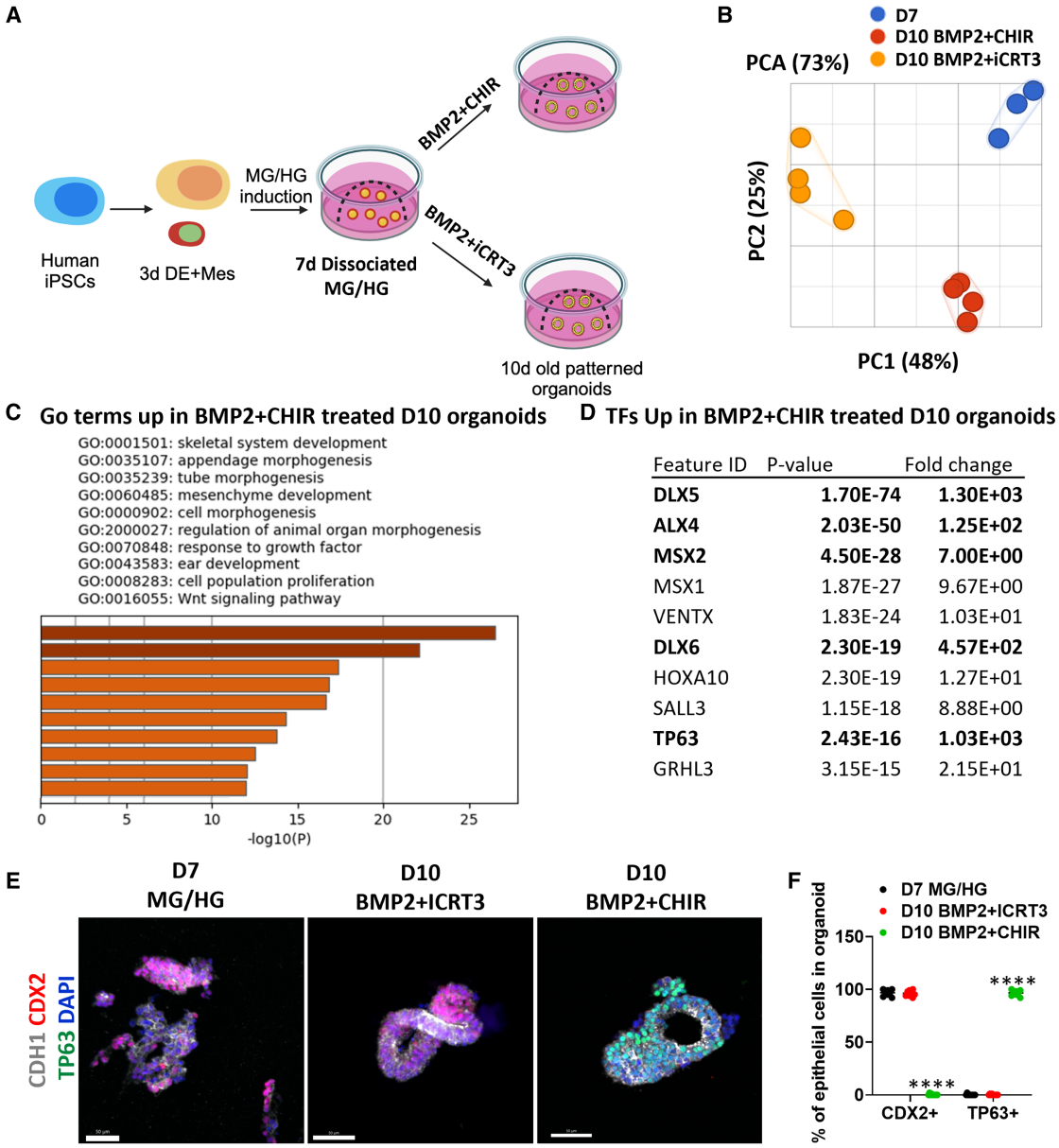

Figure 2. WNT signaling regulates lineage fate of hindgut cultures

(A) Schematic of WNT manipulation during patterning of human hindgut cultures.

(B) Principal-component analysis comparing day 7 midgut/hindgut cultures, day 10 BMP2 + ICRT3, and day 10 BMP2 + CHIR cultures. Samples were from 3 to 4 separate differentiations.

(C) Gene ontology analysis of genes upregulated in day 10 BMP2 + CHIR cultures compared to day 10 BMP2 + ICRT3 cultures.

(D–F) Table of most upregulated transcription factors in day 10 BMP2 + CHIR cultures compared to day 10 BMP2 + ICRT3 cultures. Transcription factors in (D) that overlap with those upregulated in ventral cloaca are shown in bold. Immunofluorescence staining (E) and quantification (F) of d7 and 10 cultures stained for CDH1 (white), CDX2 (red), TP63 (green) and counterstained with DAPI (blue). $N = 12$ total organoids per group, 4 organoids for each of 3 separate differentiations. Organoids were derived from the IPSC72.3 cell line. See also Figure S3, Video S1 and Table S3. Scale bars: (E) 50 μm. Data in (F) are presented as mean ± SD. **** denotes $p < 0.0001$ based on ANOVA analysis.

Transiently WNT-activated organoids maintain ventral identity and generate urothelial cell types

To determine if WNT manipulations resulted in stable specification of intestinal/colonic or urothelial tissue, we grew IPSC72.3 derived organoids to 35 days in growth media that was devoid of ICRT3 or CHIR (Figure 3A). We included a BMP2 only group to determine the effect of WNT manipulation on organoid generation. To examine the effects of WNT signaling manipulation on organoid architecture, we performed wholemount immunofluorescence staining on day 35 organoids. We used cadherin 17

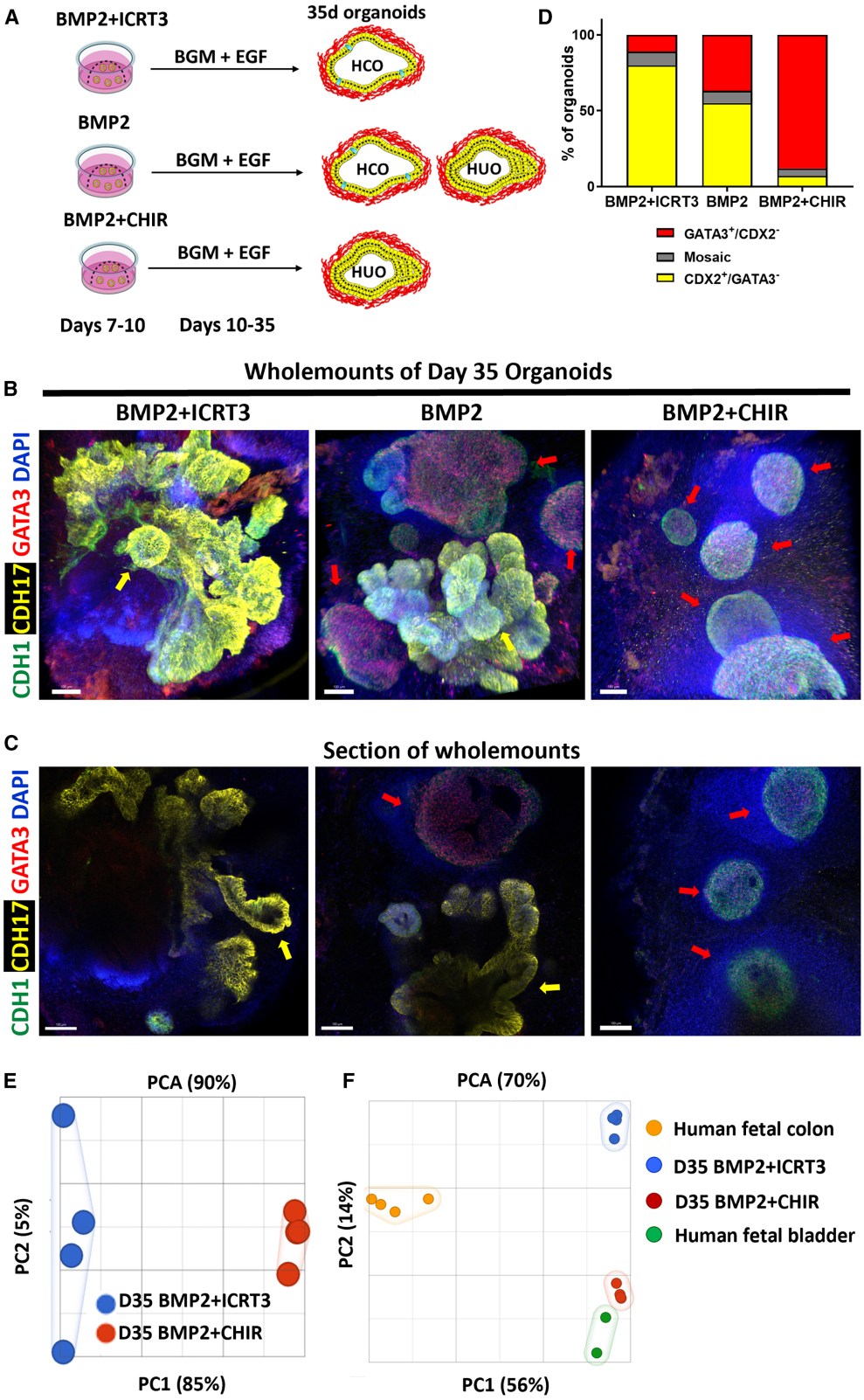

(legend on next page)

(CDH17) to mark intestinal/colonic epithelial cells and GATA3 to mark urothelial endoderm. This analysis revealed that ICRT3 treatment resulted in differentiation toward CDH17+ organoids that were composed of simple columnar epithelium and surrounding mesenchyme (Figures 3B and 3C). In addition, these organoids displayed multiple budding structures reminiscent of crypts. BMP2 treated cultures displayed a mix of organoids containing CDH17+ epithelium with budding structures or GATA3+ epithelium that formed spherical structures (Figures 3B and 3C). In contrast, activation of WNT signaling resulted in differentiation toward GATA3+ HUOs which contained stratified transitional epithelium and were spherical (Figures 3B and 3C). HUOs formed lumens that were not centrally located (Video S2). We further quantified CDX2 and GATA3 staining in sections and found the same trend as with the wholemount immunostainings (Figure 3D). We observed similar percentages of colonic, mosaic, and urothelial organoids in IPSC72.3 BMP2 treated cultures as we observed with HCO differentiations from H1 ESCs. These results indicate that WNT signaling stably promotes the generation of HUOs.

To determine the global transcriptional changes associated with WNT manipulation, we performed bulk RNA-seq on 35-day-old IPSC72.3 derived organoids. PCA revealed that BMP2+ICRT3 treated cultures clustered separately from BMP2 +CHIR treated cultures (Figure 3E). To broadly interrogate the tissue identity of BMP2+ICRT3 and BMP2+CHIR treated cultures we compared them with published datasets of human fetal large intestine and human fetal bladder. PCA revealed that primary tissues isolated from fetal bladder and our organoids clustered together along principal component 1 (PC1) axis, which accounted for 56% of the cumulative variation among samples (Figure 3F), reflecting the persistence of a minor population (11%) of HUOs in BMP2+ICRT3 treated cultures (Figure 3D). The second principal component (PC2) which accounts for 14% of the cumulative variation, revealed that BMP2+ICRT3 treated cultures clustered closer to human fetal large intestine and BMP2+CHIR treated cultures clustered closer to human fetal bladder (Figure 3F). Examination of genes that were upregulated in response to WNT inhibition revealed that BMP2+ICRT3 treated cultures were enriched in the fetal large intestinal transcriptomic signature which included the expression of the pan-intestinal transcription factors *CDX1* and *CDX2*,[28] as well as the colon specific transcription factor FXYD domain containing ion transport regulator 2 (FXYD2)[42] (Figure S4A, Tables S4 and S5). In contrast, BMP2+CHIR treated cultures were enriched in a fetal bladder transcriptional signature which included the transcription factors *GATA3*,[43,44] *GRHL3*,[38] and *TP63*[24] (Figure S4B, Tables S4 and S5). These results confirm that transient BMP2 +ICRT3 treatment stably maintains the differentiation of mid/hindgut cultures toward intestine and that transient BMP2 +CHIR treatment stably promotes the differentiation of hindgut cultures into urothelium.

We next used hypergeometric means test to determine the probability that BMP2+ICRT3 and BMP2+CHIR organoids share similar patterns of tissue-specific gene expression with human fetal large intestine and bladder respectively (Figures S4C and S4D). A total of 1,875 transcripts are expressed in the human fetal large intestine (Tables S4 and S5) and in BMP2+ICRT3 treated organoids compared to human fetal bladder or BMP2 +CHIR treated organoids, a proportion that is exceedingly unlikely by chance alone ($p = 2.9 \times 10^{-299}$). Conversely, the set of genes that is up-regulated in BMP2+CHIR treated organoids is highly enriched for genes that are up-regulated in the human fetal bladder compared to human fetal large intestines (Table S5). This analysis demonstrated that BMP2+ICRT3 treated organoids approximate human fetal large intestine and BMP2+CHIR treated organoids approximate human fetal bladder. Collectively, these data indicate that HUOs accurately reflect human fetal urothelial tissue.

HUOs recapitulate mammalian urothelial development

During mouse embryonic development, the urothelium contains distinct cell types that emerge at different developmental stages and that can be distinguished based on the combinatorial expression of markers.[1,18,45] Transient P cells (Foxa2$^+$ Upk$^+$ Isl1$^+$ P63$^+$ Shh$^+$ Krt5$^-$) dominate between E11 and E13. By E14, I cells (Foxa2$^-$ Upk$^+$ P63$^+$ Shh$^+$ Krt5$^-$) K5-BCs (Foxa2$^-$ Upk$^-$ P63$^+$ Shh$^+$ Krt5$^+$) and immature S-cells (Foxa2$^-$ Upk$^+$ P63$^-$ Shh$^-$ Krt5$^-$) emerge (Figure 4A). To determine if IPSC72.3 derived HUOs underwent similar transitions, we examined HUOs (BMP2 +CHIR cultures) at 10, 21, and 35 days. Based on prior work on HIOs, these time points are equivalent to e9-10, e12-13, and e16-18, respectively.[41] Analysis of FOXA2 and ISL LIM homeobox 1 (ISL1) revealed that most endodermal cells in day 10 HUOs were FOXA2$^+$/ISL1$^+$ (Figures 4B and 4E). Interestingly, FOXA2 expression was decreased at day 21 while ISL1 expression remained high (Figures 4C and 4E). By day 35, ISL1 expression was restricted to the basal layer of the epithelium and in the surrounding mesenchyme (Figures 4D and 4E). P63 expression was uniform at day 10, though we did not observe expression of UPK2 (Figures 4F and 4I). At day 21, we found P63$^+$/UPK2$^+$ positive cells indicating the presence of I cells and a small proportion (~4%) of UPK2$^+$/P63$^-$ S-cells, which increased to ~13% at day 35. (Figures 4G–4I). KRT5$^+$ which marks K5-BCs and KRT20$^+$ which marks S-cells were only present in 35-day old organoids in distinct populations of cells (Figures 4J–4M and S4E, Video S3). In addition, marker of proliferation Ki-67 (KI67) expression, which marks actively cycling cells, was

Figure 3. WNT patterned hindgut cultures maintain urothelial identity

(A) Schematic of long-term growth of BMP2 + CHIR cultures and BMP2 + ICRT3 cultures to 35 days.

(B) Wholemount immunofluorescence staining of 35-day old organoids for CDH1 (green), CDH17 (yellow), GATA3 (red) and counterstained with DAPI (blue).

(C) Sections from wholemounts in (B). Yellow arrows in (B and C) point to simple columnar epithelium while red arrows point to stratified transitional epithelium.

(D) Quantification of organoids stained for CDX2 and GATA3. *N* = 41 for BMP2+ICRT3, *N* = 38 for BMP2, *N* = 41 for BMP2 + CHIR.

(E) Principal-component analysis comparing day 35 BMP2 + ICRT3, and day 35 BMP2 + CHIR cultures. Samples from 4 separate differentiations are shown.

(F) Principal-component analysis comparing day 35 cultures (*N* = 4 per condition), human fetal colon (*N* = 4), and human fetal bladder (*N* = 2). Organoids were derived from the IPSC72.3 cell line. See also Figures S4 and S5, Tables S4 and S5 and Video S2. Scale bars: (B and C) 100 μm.

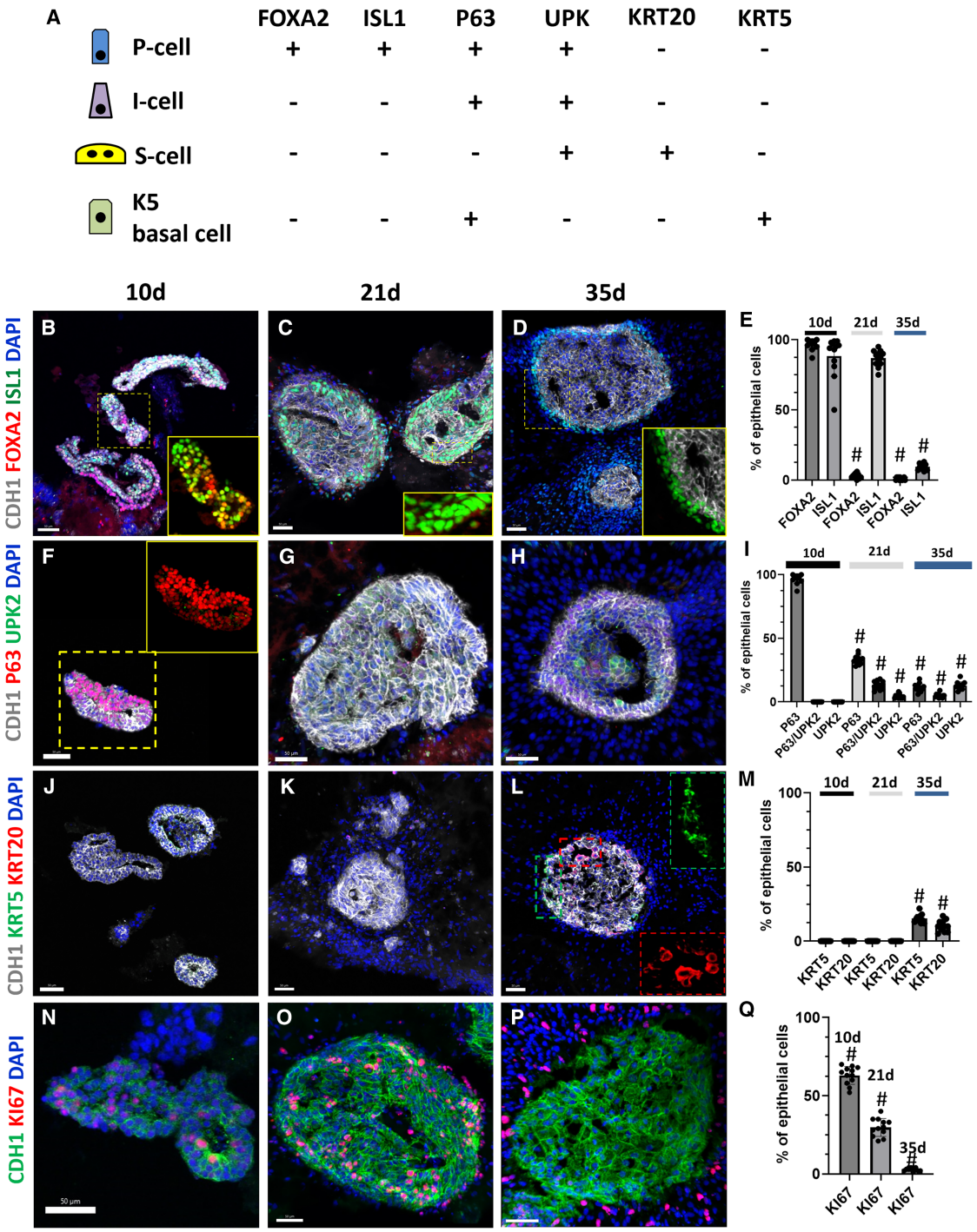

Figure 4. Urothelial cell type emergence in HUOs resembles murine fetal development

(A) Schematic depicting cell types and their associated markers during development of murine urothelium.

(B–Q) Immunofluorescence staining and quantification of 10, 21, and 35-day-old BMP2 + CHIR (HUO) cultures stained for (B–E) CDH1 (white), FOXA2 (red), ISL1 (green), (F–I) CDH1 (white), P63 (red), UPK2 (green), (J–M) CDH1 (white), KRT5 (green), KRT20 (red), (N–Q) CDH1 (green), KI67 (red). (B–D, F–H, J–L, N and O) Samples were counterstained with DAPI (blue). (N′) and (O′) have DAPI excluded. Images are representative of 4 organoids per differentiation from 3 separate differentiations. Organoids were derived from the IPSC72.3 cell line. See also Figure S4 and Video S3. Scale bars: (B–D, F–H, J–L, N, and O) 50 μm. Data in (E, I, M, and Q) are presented as mean ± SD.

# denotes $p < 0.0001$ based on ANOVA analysis.

dramatically decreased in epithelium as the organoids aged (Figures 4N–4Q). In contrast, KI67+ stromal cells were still abundant at day 35 (Figures 4P and 4Q). At 35 days, HUOs expression of KRT5, KRT7, KRT13, and TP63 was also evident (Figures S4E and S4F). In addition, 35-day-old HCOs displayed intact barrier integrity with 88% of HUOs impermeable to FITC-dextran diffusion, which decreased to 11% following ethylenediaminetetraacetic acid (EDTA) treatment (Figures S4G and S4H). Collectively these results indicate that WNT activation promotes the differentiation of hindgut cultures into urothelial progenitors that sequentially transition through distinct developmental stages, ultimately giving rise to urothelium expressing markers of basal, intermediate, and superficial cell populations.

To further characterize the cellular composition of 35-day-old HUOs, we performed immunostaining for additional mesenchymal and urothelial markers. Staining for E-cadherin (CDH1), desmin (DES), and vimentin (VIM) revealed that organoids were organized into distinct epithelial (CDH1+) and mesenchymal layers that were marked by desmin and vimentin (Figure S5A). Immunofluorescence staining for UPK2 (Figures 5A, S5B, and S5C) and UPK3 (Figure 5B) revealed the presence of S-cells lining the HUO lumen. KRT5$^-$/P63$^-$/ZO-1$^+$ S-cells were also found lining the organoid lumens (Figure 5C, S5D, and S5E). We also identified KRT5$^+$/P63$^+$/KRT20$^-$ basal cells, KRT5$^-$/P63$^+$/KRT20$^-$ intermediate cells, and KRT5$^-$/P63$^-$/KRT20$^+$ S-cells present in HUOs (Figure 5D, Video S3). Taken together, these results indicate 35-day-old HUOs undergo stereotypical urothelial differentiation and contain basal K5-cells, KRT20/ZO-1 expressing S-cells and intermediate cells.

DISCUSSION

Lineage tracing studies have demonstrated that the colorectum, bladder, and prostate all develop from common hindgut progenitors.[25] Therefore, the presence of urothelial organoids in HCO cultures reflects the common origin of colorectal and urothelial tissues. Multiple studies have reported the generation of urothelium from human pluripotent stem cells,[46–49] although only one of these protocols generated stratified urothelium.[46] However, none of these studies generated 3-dimensional organoids with co-developing mesenchyme. Furthermore, generation of stratified urothelium required the growth of urothelial cells on transwells with the addition of the combination of the peroxisome proliferator activated receptor gamma (PPAR-γ) agonist troglitazone, the epidermal growth factor receptor (EGFR) inhibitor PD153035, and fibroblast growth factor 10 (FGF10).[46] Generation of human bladder organoids from patient biopsies has been reported, however these organoids are composed of bladder progenitors and lack expression of genes associated with differentiated cell types such uroplakins or KRT20.[50] In contrast, our HUOs generated stratified urothelial tissue that contains progenitors and differentiated cells concurrently, indicating that HUOs are a suitable model for examining basal to luminal differentiation of urothelial progenitors and that HUO cultures endogenously supply the factors that are required for stratification of the urothelium. Human bladder assembloids have been generated through the combination of human bladder organoids, bladder fibroblasts, pluripotent stem cell derived smooth muscle cells, and a human microvascular endothelial cell line HULEC.[51] Although these assembloids remarkably mimic human *in vivo* bladder, the process for generating assembloids requires the growth of multiple cell types simulataneously and HULEC cells would be genetically mismatched from the other assembloid components.

Our results demonstrate the presence of KRT5 expressing cells in our human hindgut cultures. In both murine models and in human pluripotent stem cell cultures, the origin of basal cells in the urothelium remains unknown. In mice, the appearance of basal cell populations coincides with increased urinary outflow in mouse embryos,[52] and it has been suggested that this stress stimulus might regulate the appearance or expansion of these cells.[45] Urothelium within our human hindgut cultures display maturation and KRT5 expressing cells are only present in 37-day-old organoids. Our findings suggest that the appearance of these cells is intrinsically regulated in our organoid cultures. However, urinary flow may enhance the numbers of KRT5 expressing cells that appear, since the percentage of KRT5+ cells in our cultures are a fraction of those that are observed in mice at the corresponding developmental stage.[18] Examination of multiple time points between day 22 and day 37 should allow us to elucidate the signaling pathways and transcriptional programs that are involved in the generation of KRT5 expressing basal cells.

Multiple studies have implicated WNT signaling in urothelial development.[53–56] Interestingly, a previous Genome-Wide Association Study (GWAS) identified duplications in the WNT inhibitor dickkopf WNT signaling pathway inhibitor 4 (*DKK4*) in patients with ARMs.[57] Our results indicate that WNT signaling promotes the differentiation of hindgut progenitors toward urothelial fate. Therefore, CDX2/GATA3/TP63 co-staining could reveal if ARMs caused by WNT signaling modulation (or other factors) are a result of expanded ventral or dorsal cloacal progenitors. For instance, we would predict that patients with mutations in DKK4 would exhibit expansion of the GATA3/TP63 domain into the dorsal portion of the cloaca. Interestingly, loss of CDX2, and ectopic expression of GATA3 were reported in the rectum of a fetus with urorectal septum malformation sequence (URSM)[58] suggesting that the maintenance of the CDX2 and GATA3 boundary may be important for proper septation.

The septation of the cloaca into UGS and colorectum resembles the septation of the esophagus and trachea from a common foregut tube. Consistent with this observation, genetically engineered mice with perturbed sonic hedgehog,[59] or WNT[60] signaling have defects in septation of the esophagus and trachea as well as defects in the septation of the cloaca into UGS and colorectum.[53,61] Furthermore, tracheoesophageal fistula and anorectal malformations occur in conjunction with one another in human VATER syndrome (vertebral, anorectal, tracheoesophageal, renal).[62] Septation of the esophagus and trachea in mice requires the dorsoventral patterning and specification of the common foregut tube into a dorsal SRY-box transcription factor 2 (Sox2) expressing esophageal domain and a ventral NK2 homeobox 1 (Nkx2.1) expressing tracheal domain.[63] Our results suggest that the cloaca may be patterned along the dorsal-ventral axis in a similar manner, with WNT signaling inducing the TP63/GATA3 expression

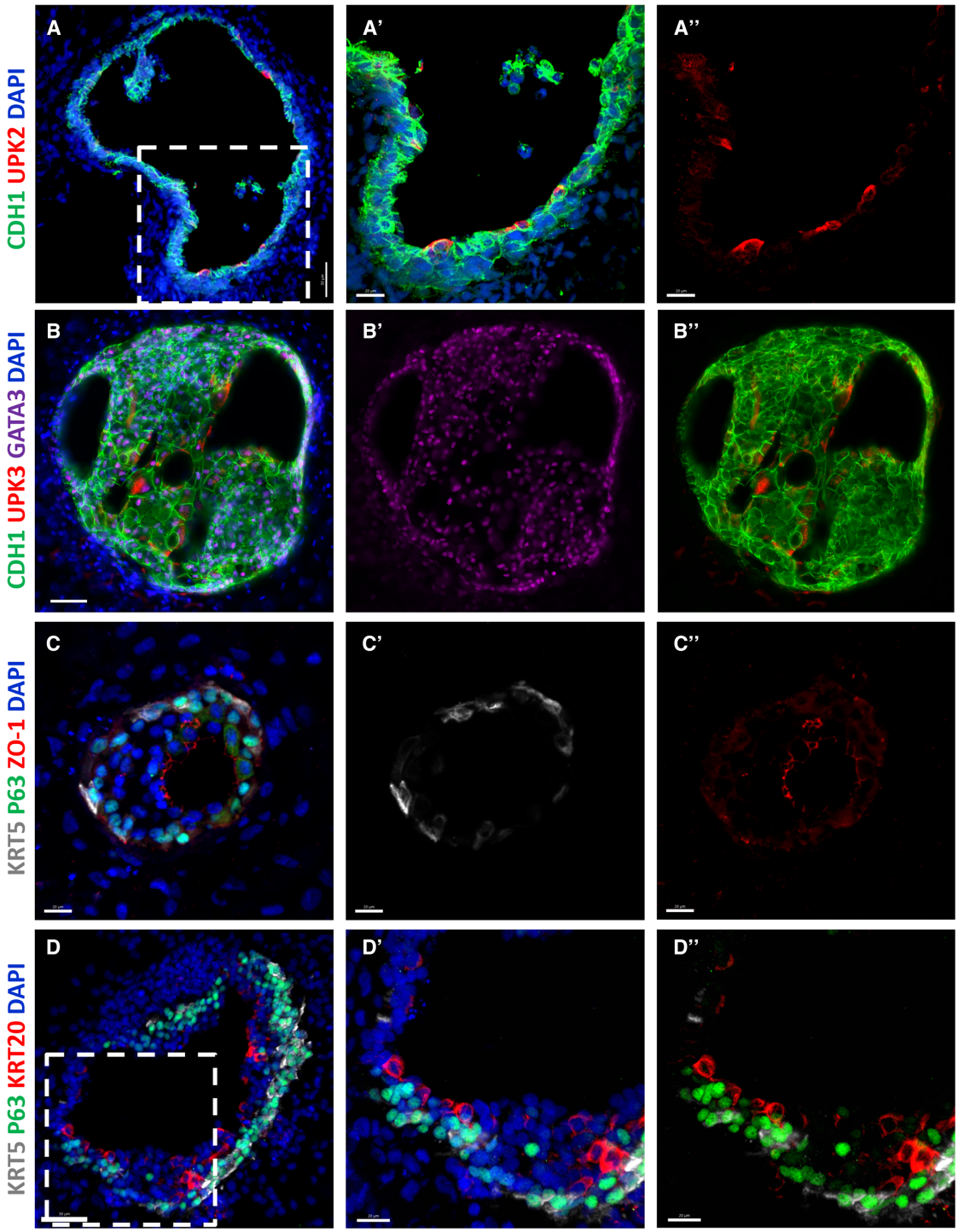

Figure 5. HUOs generate stratified layers of basal, intermediate, and superficial cells

(A) Immunofluorescence staining of 35-day old BMP2 + CHIR (HUO) cultures stained for (A) CDH1 (green) and UPK2 (red). (A′) and (A″) show higher magnification images of the boxed region in (A).

(B) Staining of CDH1 (green), UPK3 (red) and GATA3 (magenta). (B′) shows GATA3 and (B″) shows CDH1/UPK3.

(C) Staining for KRT5 (white), P63 (green) and ZO-1 (red). (C′) and (C″) show individual channels for KRT5 and ZO-1 respectively.

(D) Staining for KRT5 (white), P63 (green) and KRT20 (red). (D′) and (D″) show higher magnification images of the boxed region in (D).

(A–D) Samples were counterstained with DAPI (blue). Images are representative of 4 organoids per differentiation from 3 separate differentiations. Organoids were derived from the IPSC72.3 cell line. See also Figure S5 and Video S3. Scale bars: (A, B, B′, B″, and D) 50 μm and (A′, A″, C′, C″, D′, and D″) 20 μm.

domain and inhibiting the dorsal CDX2 expression domain of the cloaca.

Limitations of the study

In this study, we find that a 3-day activation of BMP and WNT signaling patterns CDX2+ mid/hindgut cultures into urothelial organoids. However, it is not certain that TP63+ urothelial progenitors are generated directly from CDX2+ endoderm as this would require lineage tracing of day 7 CDX2+ endodermal cells. Another limitation of our study is our assays of barrier integrity. Our assays demonstrate that HUOs display barrier function in the basal layer of the urothelium. However, among the cell layers in the urothelium, the umbrella cell layer is the only one that that forms detectable tight and adherens junctions. Although microinjecting FITC-Dextran into the lumen of HUOs would allow for the assessment of barrier integrity in the umbrella cell layer, this procedure is technically challenging due to the variable size, shape, and location of the lumen in each HUO. Although we found S-cells that line the lumen of HUOs, this lining is not continuous which likely reflects the fetal nature of the system. Although HUOs resemble human urothelium, we cannot distinguish if the urothelium is bladder-like, urethra-like, or a mix of these 2 tissues. In humans, bladder and urethra can be distinguished based on morphological differences. However, there is a dearth of markers that distinguish these tissues. Finally, the 2 cell lines used in these studies were both male so sex specific differences in differentiation were not examined.

RESOURCE AVAILABILITY

Lead contact

For additional information and requests for resources, reagents, or codes, please contact Jorge Munera (munera@musc.edu).

Materials availability

All human induced pluripotent stem cells lines are available upon request with appropriate MTA and are listed in the key resources table.

Data and code availability

- All RNA-seq and scRNA-seq data have been deposited in Gene Expression Omnibus (GEO) and are publicly available as of the date of publication. Accession numbers are listed in the key resources table.
- All scRNA-seq analysis was performed in R using previously generated codes, which are referenced in the key resources table. This paper does not report original code.
- Additional information, original images, or scripts needed for further analysis are available upon request.

ACKNOWLEDGMENTS

We would like to thank Kaleigh Doyle, Avery C. Jackson, and Priti Maity for their assistance in experiments. We would like to thank the research cores at MUSC including the Cell Models Core and the Advanced Imaging Core at MUSC. This research was supported by grants from the NIH. This work was supported by NIDDK 1R56DK129575, from the MUSC COBRE CDLD (P20 GM130457) and DDRCC (P30 DK123704).

AUTHOR CONTRIBUTIONS

J.O.M. conceived the study and experimental design; N.Q. performed and analyzed experiments and co-wrote the manuscript; A.D. and C.E.C performed experiments; D.O.K performed data analysis; all authors contributed to the editing of the manuscript.

DECLARATION OF INTERESTS

The authors declare no competing interests.

DECLARATION OF GENERATIVE AI AND AI-ASSISTED TECHNOLOGIES IN THE WRITING PROCESS

During the preparation of this work the author(s) used ChatGPT to improve language and readability. After using this tool/service, the author(s) reviewed and edited the content as needed and take(s) full responsibility for the content of the publication.

STAR★METHODS

Detailed methods are provided in the online version of this paper and include the following:

- KEY RESOURCES TABLE
- EXPERIMENTAL MODEL AND STUDY PARTICIPANT DETAILS
  - Human PSC line generation and maintenance
- METHOD DETAILS
  - Directed differentiation of human PSCs into HIO, HCOs and HUOs
  - Tissue processing, immunofluorescence, and microscopy
  - RNA isolation and bulk RNA-seq sequence assembly abundance estimation
  - Single cell RNA-seq analysis
  - Assessment of barrier function
- QUANTIFICATION AND STATISTICAL ANALYSIS

SUPPLEMENTAL INFORMATION

Supplemental information can be found online at https://doi.org/10.1016/j.isci.2025.112398.

Received: February 28, 2024
Revised: October 15, 2024
Accepted: April 7, 2025
Published: April 10, 2025

REFERENCES

1. Georgas, K.M., Armstrong, J., Keast, J.R., Larkins, C.E., McHugh, K.M., Southard-Smith, E.M., Cohn, M.J., Batourina, E., Dan, H., Schneider, K., et al. (2015). An illustrated anatomical ontology of the developing mouse lower urogenital tract. Development *142*, 1893–1908. https://doi.org/10.1242/dev.117903.
2. Gupta, A., Bischoff, A., Peña, A., Runck, L.A., and Guasch, G. (2014). The great divide: septation and malformation of the cloaca, and its implications for surgeons. Pediatr. Surg. Int. *30*, 1089–1095. https://doi.org/10.1007/s00383-014-3593-8.
3. Osman, N.I., Bratt, D.G., Downey, A.P., Esperto, F., Inman, R.D., and Chapple, C.R. (2021). A Systematic Review of Surgical interventions for the Treatment of Bladder Pain Syndrome/Interstitial Cystitis. Eur. Urol. Focus *7*, 877–885. https://doi.org/10.1016/j.euf.2020.02.014.
4. Borer, J.G., Strakosha, R., Bauer, S.B., Diamond, D.A., Pennison, M., Rosoklija, I., and Khoshbin, S. (2014). Combined cystometrography and electromyography of the external urethral sphincter following complete primary repair of bladder exstrophy. J. Urol. *191*, 1547–1552. https://doi.org/10.1016/j.juro.2013.10.104.
5. Pathak, P., Ring, J.D., Delfino, K.R., Dynda, D.I., and Mathews, R.I. (2020). Complete primary repair of bladder exstrophy: a systematic review. J. Pediatr. Urol. *16*, 149–153. https://doi.org/10.1016/j.jpurol.2020.01.004.

6. Kulkarni, J.N., Pramesh, C.S., Rathi, S., and Pantvaidya, G.H. (2003). Long-term results of orthotopic neobladder reconstruction after radical cystectomy. BJU Int. *91*, 485–488. https://doi.org/10.1046/j.1464-410x.2003.04131.x.

7. Hautmann, R.E., Volkmer, B., Egghart, G., Frohneberg, D., Gottfried, H.W., Gschwend, J., Hefty, R., Kleinschmidt, K., Küfer, R., Miller, K., et al. (2021). Functional Outcome and Complications following Ileal Neobladder Reconstruction in Male Patients without Tumor Recurrence. More than 35 Years of Experience from a Single Center. J. Urol. *205*, 174–182. https://doi.org/10.1097/JU.0000000000001345.

8. Martinez-Pineiro, L., Djakovic, N., Plas, E., Mor, Y., Santucci, R.A., Serafetinidis, E., Turkeri, L.N., Hohenfellner, M., and European Association of, U. (2010). EAU Guidelines on Urethral Trauma. Eur. Urol. *57*, 791–803. https://doi.org/10.1016/j.eururo.2010.01.013.

9. Morey, A.F., Broghammer, J.A., Hollowell, C.M.P., McKibben, M.J., and Souter, L. (2021). Urotrauma Guideline 2020: AUA Guideline. J. Urol. *205*, 30–35. https://doi.org/10.1097/JU.0000000000001408.

10. Munera, J.O., Kechele, D.O., Bouffi, C., Qu, N., Jing, R., Maity, P., Enriquez, J.R., Han, L., Campbell, I., Mahe, M.M., et al. (2023). Development of functional resident macrophages in human pluripotent stem cell-derived colonic organoids and human fetal colon. Cell Stem Cell *30*, 1434–1451,e1439. https://doi.org/10.1016/j.stem.2023.10.002.

11. Tiso, N., Filippi, A., Pauls, S., Bortolussi, M., and Argenton, F. (2002). BMP signalling regulates anteroposterior endoderm patterning in zebrafish. Mech. Dev. *118*, 29–37.

12. Wills, A., Dickinson, K., Khokha, M., and Baker, J.C. (2008). Bmp signaling is necessary and sufficient for ventrolateral endoderm specification in Xenopus. Dev. Dyn. *237*, 2177–2186. https://doi.org/10.1002/dvdy.21631.

13. Sherwood, R.I., Maehr, R., Mazzoni, E.O., and Melton, D.A. (2011). Wnt signaling specifies and patterns intestinal endoderm. Mech. Dev. *128*, 387–400. https://doi.org/10.1016/j.mod.2011.07.005.

14. Roberts, D.J., Johnson, R.L., Burke, A.C., Nelson, C.E., Morgan, B.A., and Tabin, C. (1995). Sonic Hedgehog Is an Endodermal Signal Inducing Bmp-4 and Hox Genes during Induction and Regionalization of the Chick Hindgut. Development *121*, 3163–3174.

15. Kumar, M., Jordan, N., Melton, D., and Grapin-Botton, A. (2003). Signals from lateral plate mesoderm instruct endoderm toward a pancreatic fate. Dev. Biol. *259*, 109–122. https://doi.org/10.1016/S0012-1606(03)00183-0.

16. Uhlen, M., Bjorling, E., Agaton, C., Szigyarto, C.A.-K., Amini, B., Andersen, E., Andersson, A.-C., Angelidou, P., Asplund, A., Asplund, C., et al. (2005). A human protein atlas for normal and cancer tissues based on antibody proteomics. Molecular & cellular proteomics : MCP *4*, 1920–1932.

17. Moll, R., Franke, W.W., Schiller, D.L., Geiger, B., and Krepler, R. (1982). The catalog of human cytokeratins: patterns of expression in normal epithelia, tumors and cultured cells. Cell *31*, 11–24. https://doi.org/10.1016/0092-8674(82)90400-7.

18. Gandhi, D., Molotkov, A., Batourina, E., Schneider, K., Dan, H., Reiley, M., Laufer, E., Metzger, D., Liang, F., Liao, Y., et al. (2013). Retinoid signaling in progenitors controls specification and regeneration of the urothelium. Dev. Cell *26*, 469–482. https://doi.org/10.1016/j.devcel.2013.07.017.

19. Liu, C., Tate, T., Batourina, E., Truschel, S.T., Potter, S., Adam, M., Xiang, T., Picard, M., Reiley, M., Schneider, K., et al. (2019). Pparg promotes differentiation and regulates mitochondrial gene expression in bladder epithelial cells. Nat. Commun. *10*, 4589. https://doi.org/10.1038/s41467-019-12332-0.

20. Lin, C., Yin, Y., Long, F., and Ma, L. (2008). Tissue-specific requirements of beta-catenin in external genitalia development. Development *135*, 2815–2825. https://doi.org/10.1242/dev.020586.

21. Guo, C., Sun, Y., Guo, C., MacDonald, B.T., Borer, J.G., and Li, X. (2014). Dkk1 in the peri-cloaca mesenchyme regulates formation of anorectal and genitourinary tracts. Dev. Biol. *385*, 41–51. https://doi.org/10.1016/j.ydbio.2013.10.016.

22. Baranowska Korberg, I., Hofmeister, W., Markljung, E., Cao, J., Nilsson, D., Ludwig, M., Draaken, M., Holmdahl, G., Barker, G., Reutter, H., et al. (2015). WNT3 involvement in human bladder exstrophy and cloaca development in zebrafish. Hum. Mol. Genet. *24*, 5069–5078. https://doi.org/10.1093/hmg/ddv225.

23. Miyagawa, S., Moon, A., Haraguchi, R., Inoue, C., Harada, M., Nakahara, C., Suzuki, K., Matsumaru, D., Kaneko, T., Matsuo, I., et al. (2009). Dosage-dependent hedgehog signals integrated with Wnt/beta-catenin signaling regulate external genitalia formation as an appendicular program. Development *136*, 3969–3978. https://doi.org/10.1242/dev.039438.

24. Ince, T.A., Cviko, A.P., Quade, B.J., Yang, A., McKeon, F.D., Mutter, G.L., and Crum, C.P. (2002). p63 Coordinates anogenital modeling and epithelial cell differentiation in the developing female urogenital tract. Am. J. Pathol. *161*, 1111–1117. https://doi.org/10.1016/S0002-9440(10)64387-8.

25. Pignon, J.C., Grisanzio, C., Geng, Y., Song, J., Shivdasani, R.A., and Signoretti, S. (2013). p63-expressing cells are the stem cells of developing prostate, bladder, and colorectal epithelia. Proc. Natl. Acad. Sci. USA *110*, 8105–8110. https://doi.org/10.1073/pnas.1221216110.

26. Chia, I., Grote, D., Marcotte, M., Batourina, E., Mendelsohn, C., and Bouchard, M. (2011). Nephric duct insertion is a crucial step in urinary tract maturation that is regulated by a Gata3-Raldh2-Ret molecular network in mice. Development *138*, 2089–2097. https://doi.org/10.1242/dev.056838.

27. Gao, N., White, P., and Kaestner, K.H. (2009). Establishment of intestinal identity and epithelial-mesenchymal signaling by Cdx2. Dev. Cell *16*, 588–599. https://doi.org/10.1016/j.devcel.2009.02.010.

28. Silberg, D.G., Swain, G.P., Suh, E.R., and Traber, P.G. (2000). Cdx1 and cdx2 expression during intestinal development. Gastroenterology *119*, 961–971. https://doi.org/10.1053/gast.2000.18142.

29. Pabst, O., Schneider, A., Brand, T., and Arnold, H.H. (1997). The mouse Nkx2-3 homeodomain gene is expressed in gut mesenchyme during pre- and postnatal mouse development. Dev. Dyn. *209*, 29–35. https://doi.org/10.1002/(SICI)1097-0177(199705)209:1<29::AID-AJA3>3.0.CO;2-Z.

30. Pabst, O., Zweigerdt, R., and Arnold, H.H. (1999). Targeted disruption of the homeobox transcription factor Nkx2-3 in mice results in postnatal lethality and abnormal development of small intestine and spleen. Development *126*, 2215–2225.

31. Lillevali, K., Haugas, M., Matilainen, T., Pussinen, C., Karis, A., and Salminen, M. (2006). Gata3 is required for early morphogenesis and Fgf10 expression during otic development. Mech. Dev. *123*, 415–429. https://doi.org/10.1016/j.mod.2006.04.007.

32. Raid, R., Krinka, D., Bakhoff, L., Abdelwahid, E., Jokinen, E., Kärner, M., Malva, M., Meier, R., Pelliniemi, L.J., Ploom, M., et al. (2009). Lack of Gata3 results in conotruncal heart anomalies in mouse. Mech. Dev. *126*, 80–89. https://doi.org/10.1016/j.mod.2008.10.001.

33. Grote, D., Boualia, S.K., Souabni, A., Merkel, C., Chi, X., Costantini, F., Carroll, T., and Bouchard, M. (2008). Gata3 acts downstream of beta-catenin signaling to prevent ectopic metanephric kidney induction. PLoS Genet. *4*, e1000316. https://doi.org/10.1371/journal.pgen.1000316.

34. Grote, D., Souabni, A., Busslinger, M., and Bouchard, M. (2006). Pax 2/8-regulated Gata 3 expression is necessary for morphogenesis and guidance of the nephric duct in the developing kidney. Development *133*, 53–61. https://doi.org/10.1242/dev.02184.

35. McCracken, K.W., Catá, E.M., Crawford, C.M., Sinagoga, K.L., Schumacher, M., Rockich, B.E., Tsai, Y.H., Mayhew, C.N., Spence, J.R., Zavros, Y., and Wells, J.M. (2014). Modelling human development and disease in pluripotent stem-cell-derived gastric organoids. Nature *516*, 400–404. https://doi.org/10.1038/nature13863.

36. Hentsch, B., Lyons, I., Li, R., Hartley, L., Lints, T.J., Adams, J.M., and Harvey, R.P. (1996). Hlx homeo box gene is essential for an inductive tissue interaction that drives expansion of embryonic liver and gut. Genes Dev. *10*, 70–79. https://doi.org/10.1101/gad.10.1.70.

37. Choi, M.Y., Romer, A.I., Hu, M., Lepourcelet, M., Mechoor, A., Yesilaltay, A., Krieger, M., Gray, P.A., and Shivdasani, R.A. (2006). A dynamic expression survey identifies transcription factors relevant in mouse digestive tract development. Development *133*, 4119–4129. https://doi.org/10.1242/dev.02537.

38. Gasperoni, J.G., Fuller, J.N., Darido, C., Wilanowski, T., and Dworkin, S. (2022). Grainyhead-like (Grhl) Target Genes in Development and Cancer. Int. J. Mol. Sci. *23*, 2735. https://doi.org/10.3390/ijms23052735.

39. Daniely, Y., Liao, G., Dixon, D., Linnoila, R.I., Lori, A., Randell, S.H., Oren, M., and Jetten, A.M. (2004). Critical role of p63 in the development of a normal esophageal and tracheobronchial epithelium. Am. J. Physiol. Cell Physiol. *287*, C171–C181. https://doi.org/10.1152/ajpcell.00226.2003.

40. Munera, J.O., Sundaram, N., Rankin, S.A., Hill, D., Watson, C., Mahe, M., Vallance, J.E., Shroyer, N.F., Sinagoga, K.L., Zarzoso-Lacoste, A., et al. (2017). Differentiation of Human Pluripotent Stem Cells into Colonic Organoids via Transient Activation of BMP Signaling. Cell Stem Cell *21*, 51–64.e56. https://doi.org/10.1016/j.stem.2017.05.020.

41. Spence, J.R., Mayhew, C.N., Rankin, S.A., Kuhar, M.F., Vallance, J.E., Tolle, K., Hoskins, E.E., Kalinichenko, V.V., Wells, S.I., Zorn, A.M., et al. (2011). Directed differentiation of human pluripotent stem cells into intestinal tissue *in vitro*. Nature *470*, 105–109. https://doi.org/10.1038/nature09691.

42. Gu, W., Wang, H., Huang, X., Kraiczy, J., Singh, P.N.P., Ng, C., Dagdeviren, S., Houghton, S., Pellon-Cardenas, O., Lan, Y., et al. (2022). SATB2 preserves colon stem cell identity and mediates ileum-colon conversion via enhancer remodeling. Cell Stem Cell *29*, 101–115.e10. https://doi.org/10.1016/j.stem.2021.09.004.

43. Habuka, M., Fagerberg, L., Hallström, B.M., Pontén, F., Yamamoto, T., and Uhlen, M. (2015). The Urinary Bladder Transcriptome and Proteome Defined by Transcriptomics and Antibody-Based Profiling. PLoS One *10*, e0145301. https://doi.org/10.1371/journal.pone.0145301.

44. Higgins, J.P.T., Kaygusuz, G., Wang, L., Montgomery, K., Mason, V., Zhu, S.X., Marinelli, R.J., Presti, J.C., Jr., van de Rijn, M., and Brooks, J.D. (2007). Placental S100 (S100P) and GATA3: markers for transitional epithelium and urothelial carcinoma discovered by complementary DNA microarray. Am. J. Surg. Pathol. *31*, 673–680. https://doi.org/10.1097/01.pas.0000213438.01278.5f.

45. Wiessner, G.B., Plumber, S.A., Xiang, T., and Mendelsohn, C.L. (2022). Development, regeneration and tumorigenesis of the urothelium. Development *149*, dev198184. https://doi.org/10.1242/dev.198184.

46. Suzuki, K., Koyanagi-Aoi, M., Uehara, K., Hinata, N., Fujisawa, M., and Aoi, T. (2019). Directed differentiation of human induced pluripotent stem cells into mature stratified bladder urothelium. Sci. Rep. *9*, 10506. https://doi.org/10.1038/s41598-019-46848-8.

47. Kang, M., Kim, H.H., and Han, Y.M. (2014). Generation of bladder urothelium from human pluripotent stem cells under chemically defined serum- and feeder-free system. Int. J. Mol. Sci. *15*, 7139–7157. https://doi.org/10.3390/ijms15057139.

48. Moad, M., Pal, D., Hepburn, A.C., Williamson, S.C., Wilson, L., Lako, M., Armstrong, L., Hayward, S.W., Franco, O.E., Cates, J.M., et al. (2013). A novel model of urinary tract differentiation, tissue regeneration, and disease: reprogramming human prostate and bladder cells into induced pluripotent stem cells. Eur. Urol. *64*, 753–761. https://doi.org/10.1016/j.eururo.2013.03.054.

49. Osborn, S.L., Thangappan, R., Luria, A., Lee, J.H., Nolta, J., and Kurzrock, E.A. (2014). Induction of human embryonic and induced pluripotent stem cells into urothelium. Stem Cells Transl. Med. *3*, 610–619. https://doi.org/10.5966/sctm.2013-0131.

50. Mullenders, J., de Jongh, E., Brousali, A., Roosen, M., Blom, J.P.A., Begthel, H., Korving, J., Jonges, T., Kranenburg, O., Meijer, R., and Clevers, H.C. (2019). Mouse and human urothelial cancer organoids: A tool for bladder cancer research. Proc. Natl. Acad. Sci. USA *116*, 4567–4574. https://doi.org/10.1073/pnas.1803595116.

51. Kim, E., Choi, S., Kang, B., Kong, J., Kim, Y., Yoon, W.H., Lee, H.R., Kim, S., Kim, H.M., Lee, H., et al. (2020). Creation of bladder assembloids mimicking tissue regeneration and cancer. Nature *588*, 664–669. https://doi.org/10.1038/s41586-020-3034-x.

52. Mendelsohn, C. (2009). Using mouse models to understand normal and abnormal urogenital tract development. Organogenesis *5*, 306–314. https://doi.org/10.4161/org.8173.

53. Miyagawa, S., Harada, M., Matsumaru, D., Tanaka, K., Inoue, C., Nakahara, C., Haraguchi, R., Matsushita, S., Suzuki, K., Nakagata, N., et al. (2014). Disruption of the temporally regulated cloaca endodermal beta-catenin signaling causes anorectal malformations. Cell Death Differ. *21*, 990–997. https://doi.org/10.1038/cdd.2014.21.

54. Shin, K., Lee, J., Guo, N., Kim, J., Lim, A., Qu, L., Mysorekar, I.U., and Beachy, P.A. (2011). Hedgehog/Wnt feedback supports regenerative proliferation of epithelial stem cells in bladder. Nature *472*, 110–114. https://doi.org/10.1038/nature09851.

55. Santos, C.P., Lapi, E., Martínez de Villarreal, J., Álvaro-Espinosa, L., Fernández-Barral, A., Barbáchano, A., Domínguez, O., Laughney, A.M., Megías, D., Muñoz, A., and Real, F.X. (2019). Urothelial organoids originating from Cd49f(high) mouse stem cells display Notch-dependent differentiation capacity. Nat. Commun. *10*, 4407. https://doi.org/10.1038/s41467-019-12307-1.

56. Matsumaru, D., Murashima, A., Fukushima, J., Senda, S., Matsushita, S., Nakagata, N., Miyajima, M., and Yamada, G. (2015). Systematic stereoscopic analyses for cloacal development: The origin of anorectal malformations. Sci. Rep. *5*, 13943. https://doi.org/10.1038/srep13943.

57. Wong, E.H.M., Cui, L., Ng, C.L., Tang, C.S.M., Liu, X.L., So, M.T., Yip, B.H.K., Cheng, G., Zhang, R., Tang, W.K., et al. (2013). Genome-wide copy number variation study in anorectal malformations. Hum. Mol. Genet. *22*, 621–631. https://doi.org/10.1093/hmg/dds451.

58. Huang, K.Y., Kuo, K.T., Li, Y.P., Chen, M., Yu, C.U., and Shih, J.C. (2016). Urorectal septum malformation sequence-Fetal series with the description of a new "intermediate" variant. Time to refine the terminology? Am. J. Med. Genet. *170*, 2479–2482. https://doi.org/10.1002/ajmg.a.37788.

59. Litingtung, Y., Lei, L., Westphal, H., and Chiang, C. (1998). Sonic hedgehog is essential to foregut development. Nat. Genet. *20*, 58–61. https://doi.org/10.1038/1717.

60. Harris-Johnson, K.S., Domyan, E.T., Vezina, C.M., and Sun, X. (2009). beta-Catenin promotes respiratory progenitor identity in mouse foregut. Proc. Natl. Acad. Sci. USA *106*, 16287–16292. https://doi.org/10.1073/pnas.0902274106.

61. Seifert, A.W., Bouldin, C.M., Choi, K.S., Harfe, B.D., and Cohn, M.J. (2009). Multiphasic and tissue-specific roles of sonic hedgehog in cloacal septation and external genitalia development. Development *136*, 3949–3957. https://doi.org/10.1242/dev.042291.

62. Solomon, B.D. (2011). VACTERL/VATER Association. Orphanet J. Rare Dis. *6*, 56. https://doi.org/10.1186/1750-1172-6-56.

63. Morrisey, E.E., and Hogan, B.L.M. (2010). Preparing for the first breath: genetic and cellular mechanisms in lung development. Dev. Cell *18*, 8–23. https://doi.org/10.1016/j.devcel.2009.12.010.

64. Butler, A., Hoffman, P., Smibert, P., Papalexi, E., and Satija, R. (2018). Integrating single-cell transcriptomic data across different conditions, technologies, and species. Nat. Biotechnol. *36*, 411–420. https://doi.org/10.1038/nbt.4096.

65. Hafemeister, C., and Satija, R. (2019). Normalization and variance stabilization of single-cell RNA-seq data using regularized negative binomial regression. Genome Biol. *20*, 296. https://doi.org/10.1186/s13059-019-1874-1.

66. Becht, E., McInnes, L., Healy, J., Dutertre, C.A., Kwok, I.W.H., Ng, L.G., Ginhoux, F., and Newell, E.W. (2018). Dimensionality reduction for visualizing single-cell data using UMAP. Nat. Biotechnol. *37*, 38–44. https://doi.org/10.1038/nbt.4314.

67. Qu, N., Jeffcoat, B., Maity, P., Christensen, R.K., and Múnera, J.O. (2022). Retinoic Acid Promotes the In Vitro Growth, Patterning and Improves the Cellular Composition of Human Pluripotent Stem-Cell-Derived Intestinal Organoids. Int. J. Mol. Sci. *23*, 8624. https://doi.org/10.3390/ijms23158624.

68. Gerli, M.F.M., Calà, G., Beesley, M.A., Sina, B., Tullie, L., Sun, K.Y., Panariello, F., Michielin, F., Davidson, J.R., Russo, F.M., et al. (2024). Single-cell guided prenatal derivation of primary fetal epithelial organoids from human amniotic and tracheal fluids. Nat. Med. *30*, 875–887. https://doi.org/10.1038/s41591-024-02807-z.

STAR★METHODS

KEY RESOURCES TABLE

REAGENT or RESOURCE	SOURCE	IDENTIFIER
Antibodies		
Goat anti-E-Cadherin (CDH1)	R&D Systems	Cat# AF648; RRID:AB_355504
Mouse anti-E-Cadherin	BD Transduction Lab	Cat# 610182; RRID:AB_397581
Rabbit anti-E-Cadherin (EP700Y)	Sigma-Aldrich	Cat# 246R-14; RRID:AB_1159517
Rat anti-mouse-E-Cadherin	R&D Systems	Cat# MAB7481; RRID:AB_2076679
Mouse anti-UPK3 (AU-1)	Sigma-Aldrich	Cat# 345M-14; RRID:AB_1161091
Rabbit anti-CDX2 (EPR2764Y)	Sigma-Aldrich	Cat# 235R-15; RRID:AB_1516799
Mouse anti-CDX2 (cdx-88)	BioGenex	Cat# MU392A-UC; RRID:AB_2650531
Mouse anti-human Cadherin17	R&D Systems	Cat# MAB1032; RRID:AB_2077388
Rabbit Anti-RUNX1 (EPR3099)	Abcam	Cat# ab92336; RRID:AB_2049267
Mouse anti-EPCAM	Sigma-Aldrich	Cat# 248M-94; RRID:AB_1516851
Goat anti-FOXA2	Santa Cruz Biotechnology	Cat# sc-6554; RRID:AB_2262810
Mouse anti-FOXA2	Thermo Fisher Scientific	Cat# H00003170-M12; RRID:AB_669213
Goat anti-GATA3	R&D Systems	Cat# AF2605-SP; RRID:AB_2108571
Rabbit anti-ISL1	Sigma-Aldrich	431R-14; RRID: AB_3661767
Rabbit anti-KRT13	Abcam	Cat# ab92551; RRID:AB_2134681
Rabbit anti-KRT5	Sigma-Aldrich	Cat# 305R-14; RRID:AB_1159459
Mouse anti-KRT20	Sigma-Aldrich	Cat# 320M-14; RRID:AB_1158251
Mouse anti-p63	BioGenex	Cat# AM418GP; RRID:AB_3661768
Goat anti-p63	R&D Systems	Cat# AF1916; RRID:AB_2207174
Rabbit anti-RUNX1 (EPR3099)	Abcam	Cat# ab92336; RRID:AB_2049267
Rabbit anti-UPK2	Sigma-Aldrich	Cat# HPA043312; RRID:AB_2678420
Mouse anti-ZO-1	Thermo Fisher Scientific	Cat# 33-9100; RRID:AB_2533147
Mouse anti-Desmin	Sigma-Aldrich	Cat# 243M-14; RRID:AB_1158292
Rabbit anti-Vimentin	Sigma-Aldrich	Cat# 347R-24; RRID: AB_3677338
Donkey anti-Goat Alexa Fluor 488	Thermo Fisher Scientific	Cat# A11055; RRID:AB_2534102
Donkey anti-Goat Alexa Fluor 568	Thermo Fisher Scientific	Cat# A11057; RRID:AB_2534104
Donkey anti-Mouse Alexa Fluor 488	Thermo Fisher Scientific	Cat# A21202; RRID:AB_141607
Donkey anti-Mouse Alexa Fluor 546	Thermo Fisher Scientific	Cat# A10036; RRID:AB_2534012
Donkey anti-Mouse Alexa Fluor 647	Thermo Fisher Scientific	Cat# A31571; RRID:AB_162542
Donkey anti-Rabbit Alexa Fluor 488	Thermo Fisher Scientific	Cat# A21206; RRID:AB_2535792
Donkey anti-Rabbit Alexa Fluor 546	Thermo Fisher Scientific	Cat# A10040; RRID:AB_2534016
Donkey anti-Rabbit Alexa Fluor 647	Thermo Fisher Scientific	Cat# A31573; RRID:AB_2536183
Donkey anti-Rat Alexa Fluor 488	Thermo Fisher Scientific	Cat# A21208; RRID:AB_2535794
Chemicals, peptides, and recombinant proteins		
Activin A	Cell Guidance Systems	GFH6
Accutase	Thermo Fisher Scientific	A11105-01
Advanced DMEM:F12	Thermo Fisher Scientfic	12634-010
B27 supplement w/o Vitamin A (50x) [1x]	Thermo Fisher Scientific	12587-010
Bovine serum albumin (BSA) [1%]	VWR	10842-772
Cell Recovery Solution	Corning	354253
FITC-Dextran	Sigma-Aldrich	FD4
DAPI	Sigma-Aldrich	D9542
CHIR99021 [3 μM]	ReproCell	04-0004-10

(*Continued on next page*)

Continued

REAGENT or RESOURCE	SOURCE	IDENTIFIER
ICRT3	Selleckchem	S8647
Defined fetal bovine serum (dFBS)	Hyclone	SH30070.02
Dispase	Thermo Fisher Scientific	17105-041
DMEM:F12	Thermo Fisher Scientific	11320033
Fetal bovine serum	Sigma Aldrich	12306C
HEPES Buffer	Thermo Fisher Scientific	15630080
hESC-qualified Matrigel	BD Biosciences	354277
L-glutamine (100x) [1x]	Thermo Fisher Scientific	25030-081
Matrigel Matrix Basement Membrane	BD Biosciences	354234
mTeSR1 media	Stem Cell Technologies	5850
N2 Supplement (100x) [1x]	Thermo Fisher Scientific	17502-048
Non-essential Amino Acids (100x) [1x]	Thermo Fisher Scientific	11140050
Normal donkey serum	Jackson ImmunoResearch Laboratories	017-000-121
Pen/Strep (100x)	Thermo Fisher Scientific	15140-122
recombinant human BMP2	R&D Systems	355-BM-050
recombinant human BMP4	R&D Systems	314-BP-050
recombinant human EGF	R&D Systems	236-EGF-01M
recombinant human FGF4	R&D Systems	235-F4
Y-27632 dihydrochloride	Tocris	1254
Critical commercial assays		
NucleoSpin RNA	Macherey-Nagel	740955
Deposited data		
scRNA-seq data – H1 day 22 and day 35 HCOs.	Munera et al.[10]	GEO: GSE240363
Bulk RNA-seq data – H1 day 21 and day 35 HIOs and HCOs.	Munera et al.[10]	GEO: GSE240363
Bulk RNA-seq data – e10.5 ventral and dorsal cloaca.	GUDMAP project	GEO: GSE88764
Bulk RNA-seq data – IPSC72.3 derived *in vitro* day 7, day 10 and day 35 HCOs and HUOs.	This paper	GEO: GSE259318
Experimental models: Cell lines		
Human: H1 ES cells	CCHMC Pluripotent Stem cell core / WiCell Research Institute	NIH hESC-10-0043
Human: iPSC72.3 iPS cells	CCHMC Pluripotent Stem cell core/McCracken et al.[35]	N/A
Experimental models: Organisms/strains		
Mouse: Wildtype CD1 Mice	Charles River	022
Software and algorithms		
Partek® Flow®		
IMARIS	Bitplane	N/A
NIS Elements	Nikon	N/A
R		v3.6.3, v4.1.1, and v4.2.1
R Studio		v1.2.5033 and v1.4.1717
Seurat	Butler et al.[64]	v3.2.1
CellRanger	10x Genomics	v3.0.2
SCTransform	Hafemeister et al.[65]	
UMAP	Becht et al.[66]	
Prism 9	Graphpad	v9.5.1
Image J.		

(*Continued on next page*)

Continued

REAGENT or RESOURCE	SOURCE	IDENTIFIER
Other		
Ibidi 8 well chambers	Ibidi	80286
Ce3D™ Tissue Clearing Solution	Biolegend®	427703

EXPERIMENTAL MODEL AND STUDY PARTICIPANT DETAILS

Human PSC line generation and maintenance

The human ESC (H1, WiCell, RRID: CVCL_9771) and control human iPSC line 72.3 (RRID: CVCL_A1BW) were obtained from the Cincinnati Children's Hospital Medical Center (CCHMC) Pluripotent Stem Cell Facility. H1 cells were generated from human blastocysts and iPSC 72.3 cells were derived from a donor of unspecified age. iPSC 72.3 cells were generated from foreskin fibroblasts using episomal plasmids. Both lines were derived from male donors. HPSCs were maintained in mTeSR1 (StemCell Technologies) on hESC-qualified Matrigel (Corning) coated Nunclon Delta Surface 6-well plates (Thermo Scientific). Spontaneous differentiation was manually removed and cells were passaged every 3-4 days using Dispase. Cells were authenticated and routinely confirmed to be karyotypically normal and mycoplasma negative.

METHOD DETAILS

Directed differentiation of human PSCs into HIO, HCOs and HUOs

Generation of HIOs and HCOs has been previously published.[40,41] Briefly, human ES and iPSCs were plated as single cells in mTeSR1 media plus ROCK inhibitor Y27632 (10 μM; Stemgent) on hESC-qualified Matrigel (Corning)-coated 24-well plate at 150,000 cells per well. Beginning the next day, cells were treated with Activin A (100 ng/ml; Cell Guidance Systems) for three days in RPMI 1640 (Invitrogen) containing increasing concentrations of 0%, 0.2%, and 2.0% define fetal bovine serum (dFBS; Invitrogen). For endoderm induction of iPSC72.3, BMP4 (15 ng/ml) was added to the first day of Activin A treatment. Following definitive endoderm induction, cells were treated for 4 days with FGF4 (500 ng/ml; R&D Systems) and CHIR99021 (3 μM; Stemgent) in RPMI 1640 with 2.0% dFBS to generate 3-dimensional mid-hindgut spheroids. For WNT inhibition and activation studies we used mid/hindgut monolayer that was dissociated into clumps as previously described.[67] These mid/hindgut clumps were embedded in basement-membrane Matrigel (BD Biosciences) and subsequently grown in Advanced DMEM/F12 (Invitrogen) supplemented with N2 (Invitrogen), B27 (Invitrogen), L-glutamine, 10 μM HEPES, penicillin/streptomycin, and EGF (100 ng/ml; R&D Systems). For proximal HIO and HCO specification, Noggin (100 ng/ml; R&D Systems) or BMP2 (100 ng/ml; R&D Systems) was added for the first three days of three-dimensional growth, respectively. For WNT modulation experiments, BMP2 (100 ng/ml; R&D Systems) and either ICRT3 (50μM; Selleckchem) or CHIR99021 (3 μM; Stemgent) was added for the first three days of three-dimensional growth. Organoids were transferred to new Matrigel following 2-3 weeks.

Tissue processing, immunofluorescence, and microscopy

Tissues were fixed for 0.5-1 hr in 4% paraformaldehyde (PFA) on ice. Organoids frozen in OCT. OCT sections were blocked using donkey serum (5% serum in 1× PBS plus 0.5% Triton-X) for 30 min and incubated with primary antibody overnight at 4°C. Slides were then washed 3X with 1X PBS plus 0.5% Triton-X and incubated in secondary antibody with DAPI in blocking buffer for 2 hr at room temperature (23°C). The antibodies used are listed in the key resources table. Slides were then washed 2X with 1X PBS plus 0.5% Triton-X followed by a final wash in 1X PBS. Slides were then mounted using Fluoromount-G® (SouthernBiotech). Images were captured on a Nikon A1 confocal microscope (CCHMC) or a Zeiss LSM 880 NLO confocal microscope (MUSC) and analyzed using NIS Elements (Nikon) or Imaris Imaging Software (Bitplane).

For wholemount staining of mouse embryos or organoids, fixed embryos or organoids were washed with PBS and then permeabilized in PBST overnight at 4°C on a rocking platform. Embryos or organoids were then blocked for 6-8 hours on a rocking platform, incubated in primary antibody overnight at 4°C on a rocking platform, washed 5X with PBST, incubated in secondary antibody overnight at 4°C on a rocking platform, washed 2X with PBST followed by a final wash in PBS. A set of organoids was cleared using Ce3D™ Tissue Clearing Solution (Biolegend) following the manufacturer's protocol. Alternatively, embryos or organoids were dehydrated by washing 3 times in 100% Methanol and cleared using Murray's clear (2 parts benzyl benzoate and 1 part benzyl alcohol). Images were captured on a Nikon A1 confocal microscope using Z-correction, or on a Zeiss LSM 880 NLO with Airscan confocal microscope. Images were analyzed using Imaris Imaging Software (Bitplane) or ImageJ.

RNA isolation and bulk RNA-seq sequence assembly abundance estimation

RNA was extracted using NucleoSpin® RNA extraction kit (Macharey-Nagel) according to manufacturer's protocols. RNA library construction and RNA sequencing was performed by BGI using the DNBseq platform. QC analysis was performed with data from the DNBseq platform and downstream analysis was performed using Partek® Flow® software. Heatmaps were generated using

TPM tables that were then converted into heatmaps using Morpheus (Broad Institute). H1 cell derived HIO and HCO data can be found by accession number GSE240363 . WNT inhibited or activated hindgut organoids are also from 3-4 independent differentiations done using a subclone of the IPSC72.3 line. Human fetal RNA-seq data were downloaded from GEO. Human fetal colon data can be found via the accession number GSE18927. Human fetal bladder data can be found via the accession number GSE78563.

Single cell RNA-seq analysis

We used previously published scRNA-seq data which can be found by accession number GSE240363, for our analysis. Raw scRNA-seq data was converted to FASTQ files and then aligned to the human genome [hg19 d37 HCO or hg38 for d22 HCO] using CellRanger v3.0.2 (10x Genomics). Individual analysis, including quality controls and clustering, of all datasets was first performed using Seurat [v3.2.3][64] in R [v3.6.3]. Basic filtering parameters for gene detection included greater than or equal to 3 cells and all cells with minimum 100 detected genes and maximum 7,500 genes. Percent.mito parameter was all cells less than 20. Data was normalized using SCTransform[65] in Seurat. Cell cycle effect was regressed out using previously established methods in Seurat. Normalized expression levels underwent principal component analysis (PCA) followed by uniform manifold approximation and projection (UMAP)[66] with subsequent Louvain clustering. Cluster resolution was changed to increase or decrease number of clusters identified. Datasets from two independent d22 HCO replicates were merged using Seurat prior to normalization, PCA, UMAP, and clustering. Marker genes were determined using 'FindAllMarkers' function (Wilcoxon rank-sum test). Clusters were annotated manually using unbiased methods.

Assessment of barrier function

Our barrier function studies which are modeled on a previous study,[68] examined barrier integrity of the basal epithelial layer. Organoids were isolated from Matrigel, and then resuspended in either PBS or 4mM EDTA diluted in PBS. The suspension was incubated for 15 minutes on ice. Following incubation, the solution was centrifuged, and the supernatant was removed. The organoids were then washed once with PBS. Subsequently, the organoids were resuspended in Advanced DMEM-F12, with a working concentration of FITC at 1mg/ml and incubated for 1 hour at 37°C. Following incubation, the organoids were directly imaged using a confocal microscope.

QUANTIFICATION AND STATISTICAL ANALYSIS

For experiments involving patterned mid/hindgut clumps and *in vitro* grown organoids, "n" represents the number of biological replicates (2-3 wells were collected for each replicate). Quantification of data are represented as mean ± SD unless otherwise specified. Significance was determined by either unpaired t tests with 2-tailed distribution and two-sample equal variance when comparing 2 conditions or one-way ANOVA with Tukey's multiple comparison test when comparisons >2 conditions. Significance represented as $p<0.05$*, <0.01**, $p<0.001$***, $p<0.0001$**** or # as denoted in Figure legends. Statistics were performed and graphs were generated in GraphPad Prism. All figures were generated using Adobe Illustrator.